Supporting information

Manipulating three-dimensional bending to extraordinarily stiffen two-dimensional membranes by interference colors

Yuwei Zhu,‡[1] Peng Wang,‡[a,b] Si Xiao,*[a] Song He,[a] Jiazhang Chen,[a] Yilin Jiang,[a] Yiduo Wang,[a] Jun He *[a] and Yongli Gao [a,c]

1. Extracting the gray values of R and G channels from the colored interference fringes to calculate the height at different positions of the selected line.

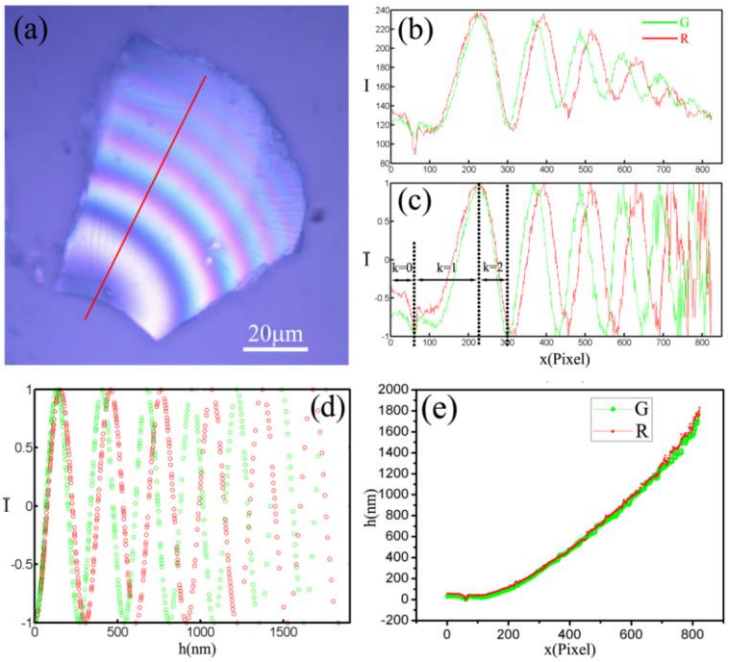

Figure.s1 procedure of obtaining the height corresponding to different positions. **(a)**Optical microscope image of a piece of MoS_2 thin film. **(b)** Extracted gray values of R and G channels respectively at the point of the red reference line in **(a)** by MATLAB software, and **(c)** relative gray values after normalization. **(d)** Height corresponding to relative intensity at R and G channels. **(e)** Height corresponding to different positions of two channels.

[1] *School of Physics and Electronics, Hunan Key Laboratory for Super-micro structure and Ultrafast Process, Central South University, 932 South Lushan Road, Changsha, Hunan 410083, P. R. China. E-mail: sixiao@csu.edu.cn, junhe@csu.edu.cn.*
[b] *Key Laboratory of Advanced Optical Communication Systems and Networks, School of Physics and Astronomy, Shanghai Jiao Tong University, Shanghai, 200240, P.R. China.*
[c] *Department of Physics and Astronomy, University of Rochester, Rochester, New York 14627, United States.*
‡These authors contributed equally to this work.

By using the white-light source, a serious of optical microscope images for the samples can be obtained. When the thickness of the gap between MoS_2 membranes and the substrate satisfies the optical interference condition, the colored interference fringes can be formed. Figure.s1(a) is the interferogram captured by a charge-coupled device (CCD). The amount of resolved stripes are about ten groups. According to the study by Brian Smits et al. [1, 3], it is possible to match the gray values of RGB channels with the wavelengths using MATLAB software. Figure.s1(b) is the extracted gray values of R and G channel respectively at the point of the red reference line from Figure.s1(a), where abscissa values represent the position of pixel in the picture.

Since the incident angle is near zero, the proposed optical interference equation is [2]:

$$I = I_1 + I_2 + 2\sqrt{I_1 I_2}\cos(\frac{4nh\pi}{\lambda} + \phi) \qquad (1)$$

Where I is the intensity of the interference light, and h is the thickness of the gap between MoS_2 membrane and the substrate. I_1 and I_2 are the intensities of two coherent beams, n is the refractive index of the medium in the gap, λ is the wavelength of the considered light and Φ is the initial phase change. I_1 and I_2 can be expressed by I_{max} and I_{min}, the maximum and minimum interference intensities, which are in the same interference order:

$$\begin{aligned} I_1 &= I_{\max} + I_{\min} + 2\sqrt{I_{\max} I_{\min}} \\ I_2 &= I_{\max} + I_{\min} - 2\sqrt{I_{\max} I_{\min}} \end{aligned} \qquad (2)$$

The relative interference intensity of any point is defined as:

$$\bar{I} = \frac{2I - I_{\max} - I_{\min}}{I_{\max} - I_{\min}} \qquad (3)$$

In Figure.s1(c), the intensities (gray value) of R and G channels are normalized based on equation (3), and $\bar{I}$ is termed as the 'relative intensity'. Since multi-level interference would appear in the same interferogram, the half-order k is introduced in the calculation process. The numeric value of k increases as the number of peaks and valleys increases, as Figure.s1(c). The first few segments of k are shown in Figure.s1(c). And the thickness h traditionally given by equation (4) [2, 4] can be written as equation (5) when taking the half-order k into account.

$$h = \frac{\lambda}{4n\pi}[\arccos(\bar{I}) - \arccos(\overline{I_0})] \quad (4)$$

$$h = \frac{\lambda}{4\pi n}[(-1)^k \arccos \bar{I} - \arccos \overline{I_0} + (k + \left|\sin \frac{k\pi}{2}\right|)\pi] \quad (5)$$

Where $\phi = \arccos(\overline{I_0})$. In fact, equation (5) would turn into equation (4) when *k* is 0. In this study, we have chosen the primary wavelength λ_R=610 nm and λ_G=540 nm (Further explanation in details is shown in Figure.s2 and Figure.s3). The refractive index of medium (air) in gap *n*=1. Figure.s1(d) presents *h*- $\bar{I}_R$ and *h*- $\bar{I}_G$ curves based on equation (5). And Figure.s1(e) can be obtained after combined Figure.s1(c) and Figure.s1(d). As *x*-*h* curves are shown in Figure.s1(e), the abscissa values (position) is extracted from Figure.s1(c) while ordinate values is extracted from Figure.s1(d). Because the two *x*-*h* curves are basically coincident with each other, R and G channel either can be used to calculate the height at any positions based on optical interferometry. For this paper, G-channel is chosen for 3D reconstruction.

2. Description and verification of λ_R=610 nm and λ_G=540 nm.

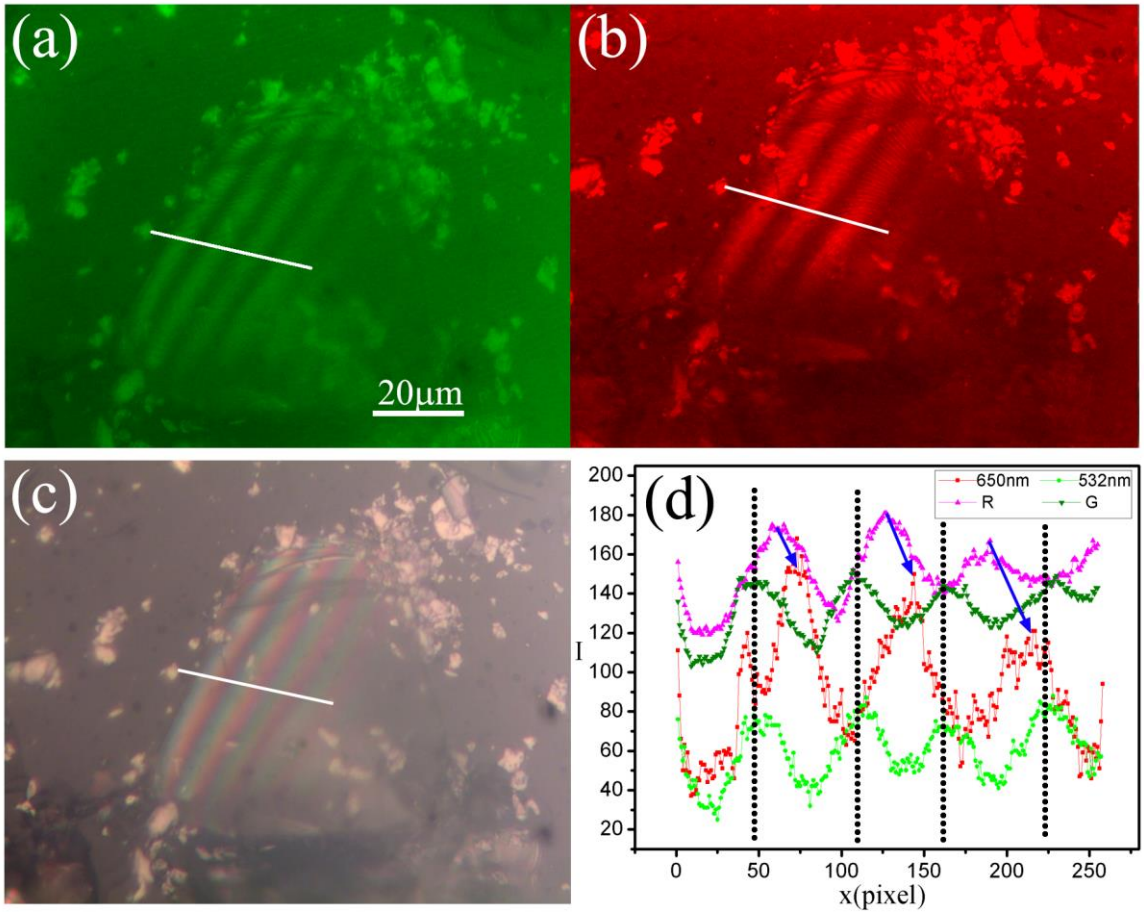

Figure.s2 (a)(b)(c) present microscope images of the same piece of MoS_2 thin film separately using 532nm, 650nm laser and the halogen light as the light source. **(d)**The extracted gray values from the location of white reference line in **(a)(b)(c)**.

The colored interference fringes were collected by a charge-coupled device (CCD) camera and the images were sent to a computer digitizing system. In order to testify that it is reasonable to choose the primary wavelength as λ_R=610 nm and λ_G=540 nm, two kinds of CW lasers with wavelength of 532 nm and 650 nm were selected as the light sources in optical microscope. Figure.s2 (a)(b) are the corresponding microscope images of MoS_2 thin film separately using 532 nm, 650 nm lasers. Figure.s2 (c) is the microscope image of the same piece using the halogen light. Figure.s2(d) shows the extracted gray values from the position of white reference line in (a)(b)(c).

The curve of '532 nm' in Figure.s2(d) is extracted from Figure.s2(a) (using 532 nm laser), and the curve of 'G' is extracted from G channel of Figure.s2(c). The curves of '532 nm' and 'G' show well agreement at the point of the peaks and valleys. 'G' offset slightly to the right, which indicates

that the center wavelength of G-channel acquired by the CCD is around 540 nm. The curve of '650 nm' in Figure.s2(d) is extracted from Figure.s2(b) (using 650 nm laser), and the curve of 'R' is extracted from R channel of Figure.s2(c). The curve of '650 nm' have a large offset to the right referring to 'R' curve, and its peaks and valleys are between '532 nm' and '650 nm' at the same order. Thus the center wavelength of R channel in this experiment is also between 532 nm and 650 nm. In Figure.s1(e), when λ_R=610 nm was chosen for calculation, *x*-*h* curves of R and G channels showed strong agreement. So that the center wavelength of R-channel is supposed to be 610 nm.

It should be noted that the acquired height values are all using G-channel (λ=540nm) in main text. And as demonstrated area in Figure.s3b and Figure.s3c, the reconstructed 3D mapping is similar to AFM detection result, and the error approaches 1%.

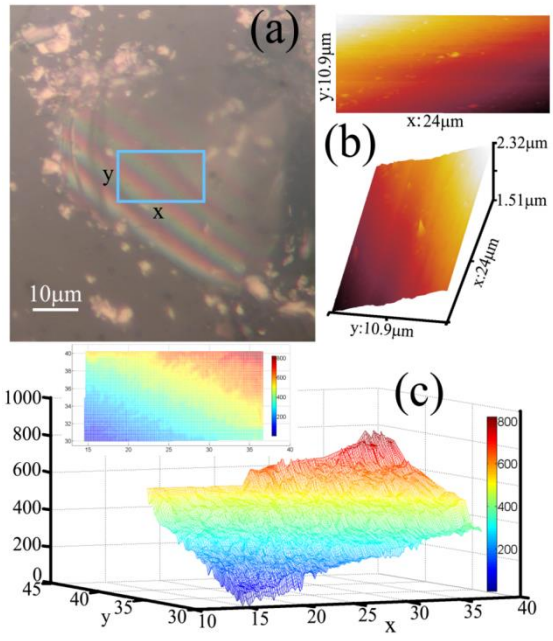

Figure.s3 The experimental and theoretical results of the selected area depicted as a blue box in **(a)**. **(a)** is the original optical microscope photograph. **(b)** is the 3D morphology in the blue-box area measured by AFM, the maximum height difference is 810 ± 2 nm. **(c)**The 3D reconstruction of the same area based on G-channel extracted from interference colors, and the calculated maximum height difference is 800 ± 5 nm. It means the error approaches 1%.

3. Schematic diagram of the setup that detection and manipulation at the same time.

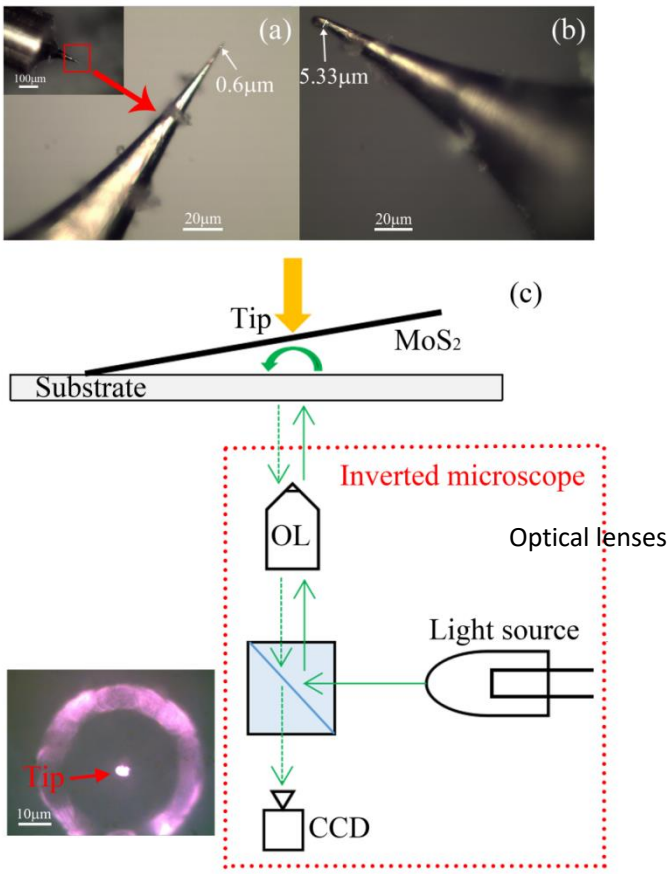

Figure.s4(a) The self-made probe by electrolytic method for micro-force operation, the diameter of tip is less than several hundred nanometers. **(b)** To prevent the MoS_2 membranes from being punctured easily by the tip, the blunt tip with its diameter up to micron order (around 5 μm) is optimal for manipulation, and it is easier to detect and mark the tip under the inverted microscope. In order to blunt the tip, the tip was stressed in contact with the hard glass slide until the spot of the tip can be clearly measured in optical microscope. **(c)**The manipulation and detection setup: the MoS_2 membranes can be manipulated by the tip, in the meantime, the morphology of the sample is detected with an inverted microscope (4XCE, Caikon Reagent Co., Ltd of Shanghai, China). The inset is the tip observed in the microscope, which presented a clearly yellow bright spot.

4. Deformation of the MoS_2 thin film under stress (see video for more details).

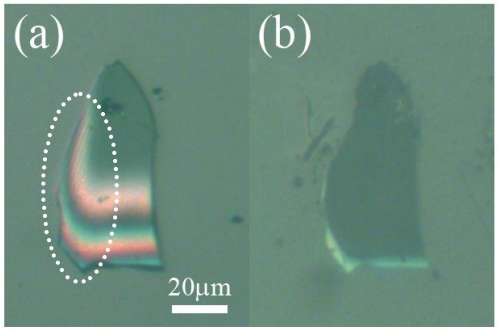

Figure.s5 (a) MoS_2 membrane was newly transferred to the substrate. The interference colors widely distributed in the surface of MoS_2 membrane. In this situation, the gap between the membranes and substrate was brimmed with Tetrahydrofuran (THF) solvent. **(b)** After annealed at 80 ℃ for about 5 hours, the liquid in the gap was completely evaporated, and interference colors almost disappeared except lower edge of the membrane.

The THF solvent used as a medium here. It is because that the THF solvent can easy volatilize. After annealing, the solvent will evaporate completely, so the impact from liquid, such as the surface tension, could be excluded. But in the next part of Figure.s8, the solvent is needed not easy to evaporate, which can be used as the "liquid-workbench" . So, The solvent such as DMF (N, N-Dimethylformamide) were chosen in Figure.s8. In addition, as we reported before, the width of gap and the bending curvature of MoS_2 membranes, can be regulated by THF solvent with a micro-surface-tension[5]. However, under the impact of the solvent evaporation or surface tension from THF, the membranes deformed slowly on hour-scale (by annealing), even day-scale (by evaporation at room emperature), but not within minute-scale. Thus, the membrane deformation (second-scale) demonstrated in Figure.s6 are all caused by the additional force from the tip.

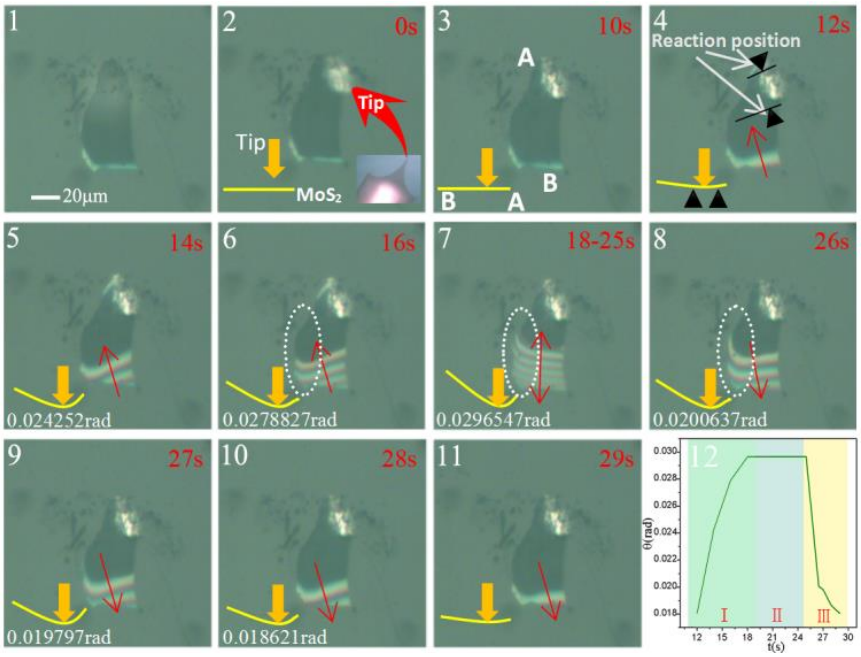

Figure.s6 shows the deformation of a piece of suspended MoS_2 membrane under external forces. **(1)** MoS_2 membrane before bearing the load. **(2)** The tip (in the inset) was positioned over the membrane. The membrane was near the focal plane of microscope objective and presenting a clear picture, while the tip was fuzzy because it is far from the surface. **(3)** It presented a clear yellow bright spot once the tip was in contact with the membranes, due to the strong scattering or reflectivity of the tip. In **(4-6)** process, as the external forces continuously increased, the fringes extended along the same direction depicted with a red arrow, result of a larger gap and growing longitudinal bending. It inferred that some micro-particles existed in the gap as fulcrums for the membrane, leading to a suspended MoS_2 membrane over the substrate. In **(4)**, it depicts two possible fulcrums of "beam model" characterized by two dark triangles, and the membrane sank where in contact with the tip, while the lower edges tilting upward. **(7)** The direction of fringes happened to deflect during lateral deviation. It means that transverse distortion had appeared. The reason is that this membrane reached the limit of its load capacity. So, we gradually reduced the external force after that moment. And **(8-11)** is the inverse process of **(4-6)**, interference colors were gradually fading as the force was decreasing. A schematic diagram at left lower corner in **(2-11)** not only shows the relative location relationship between the tip and membrane, but also the longitudinal deflection and the bent angle of cross section of the membrane at that time. As marked by white dashed box (in 8 and Figure.s5(a)), the fringes on the left side of the membrane maintained throughout all the process, such as annealed before and after(Figure.s5), or the process of increasing **(4-6)** and decreasing **(8-11)** the external forces. It indicates that the transverse curvature is natural deformation rather than the influence of external forces. **(12)** shows the time-angle curve for deformation process. Sections I(green), II(blue) and III(yellow) represent the regions of the process of increasing force, stable state, and process of

decreasing force, respectively. The interference colors deformed quickly on second-scale under an additional force from a tip.

5. Why the thick of 250 nm was chosen in experiments?

Actually, the 3D curvature could still be regulated even the thickness of MoS2 membrane exceeds 250nm. However, the isoclinic interference with narrow and black fringes would be observed as we reported before5, which influence the observable of coloured fringes resolution. So, we had not chosen the thicker membranes in order to reduce inaccuracy. It is exact to detect the curvature of the few layers membrane with thickness less than 250nm. As for manipulation, the experimental difficulty is that the monolayer or fewer layers membranes are too flexible, leading to unrecoverable destruction by the tip used in present work due to their small bending rigidity. The optical tweezers would contribute to manipulate the structures of monolayer and fewer layers 2D membranes.

Under the experimental condition in our lab, multy-layer MoS_2 thin films with thickness between 50-250nm can be prepared by solvent-based exfoliation method, since they would have a similar mechanical behave with 250nm membrane. However, we should admit that it is much more convenient to manipulate membrane with larger dimension, whereas dimension usually proportional to thickness. So, the preparation parameters were adjusted to choose the most suitable thick(250nm) of MoS_2 membrane, which contribute to the manipulating process and monitoring progress.

6. The process of loading and detecting the micro-force.

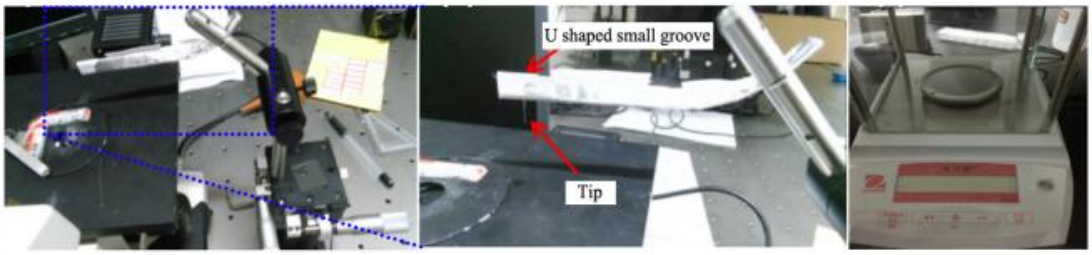

Figure.s7 Snapshot of the force loading **(a, b)** and detecting system**(c)**.

The system is a combination of two different parts: the force loading system and the detecting system. The force loading system is shown in Figure.s7**(a, b)**. The main part is a manually-operated three-axis micrometer stage, which can globally locate the probe. A cantilever made of tin-foil is fixed on the stage, while the probe is fixed on the cantilever. The detecting system (c) is a commercial electronic micro-balance (AW220) with 20g capacity and 0.01mg resolution. Besides, the load used in the experiment is Fe_3O_4 magnetic powder with micro particles, the density is about 5.18 g/cm^3.

The experimental process is as followed: Firstly, the probe was lowered until it exactly touched the surface of the sample. So that the tip visibly presented as a yellow bright spot in the optical microscope. Then, the micro particles (Fe_3O_4 magnetic powder) were taken onto the small U-shaped

grooves gradually, which was hanging on the cantilever. The deadweight of particles led the cantilever downward for an increment. So that the tip, which was mounted on the cantilever, pressed down the MoS_2 membrane to manipulate the gap. And the changes of gap would influence the distribution of interference colors, that could be observed by optical microscope. Finally, in order to quantitatively measure the load, the MoS_2 membrane was replaced by the weighing pan of an electronic micro-balance. Thus, in terms of the digital readout provided by electronic micro-balance, the force could be measured and recorded.

But there are some defects and deviations remained in this system: (1) The deformation of the probe when contacting with the weighing pan was ignored, and the stiffness of the balance was supposed to be theoretically infinite so that the weighing pan rebounded back to original plane; (2) The mechanical properties of tin-foil cantilever was still unclear, and it is not sure whether it had distortion in horizontal direction when bent in vertical direction. And the uncertainty attained in this system was estimated to be less than 2% [6].

7. Manipulation of MoS_2 membrane bending degrees (see video for more details).

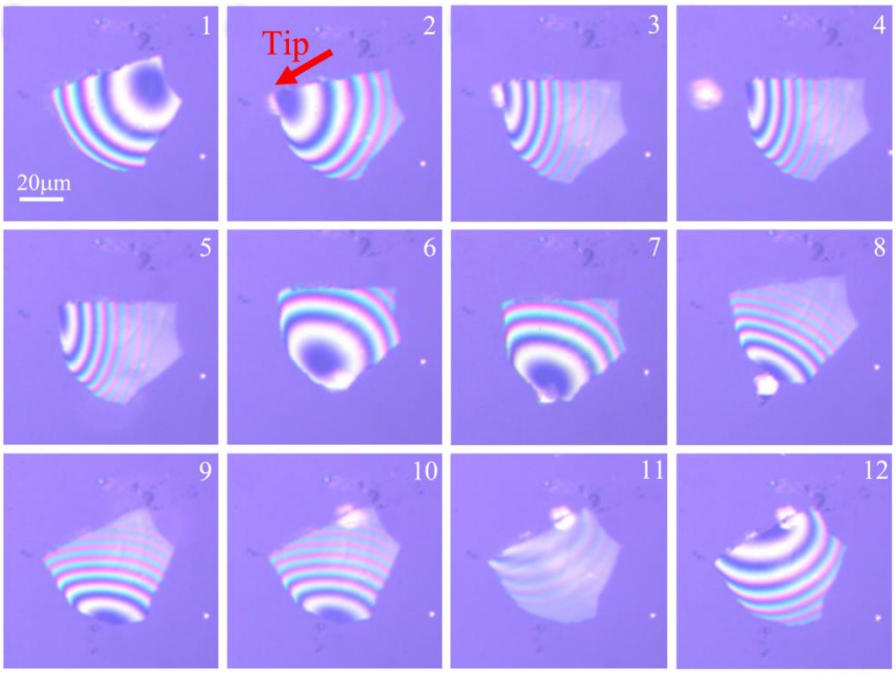

Figure.s8 were three different processes to manipulate the distribution of interference fringes. The yellow bright spot was represented the tip. Figure.s8**(1)**, The interference colors was spreading all over the MoS_2 membrane, due to the micro-droplet as a workbench between the membrane and substrate. Figure.s8**(2, 3)** showed that the interference colors of the whole region could be detected and manipulated at the same time. Figure.s8**(4, 5)**, after the tip was separated from the surface of

membrane, the interference colors can maintain stable. Figure.s8**(6-9)** showed the second touching process at the different point. The bending orientation was rotated about 90° while the membrane remained stable. Figure.s8**(10-12)** was another process to rotate the bending orientation of the membrane about 180°. In addition, the 3D curvatures of membrane were also changed in each process, which can be calculated based on the interference colors in Figure.s10.

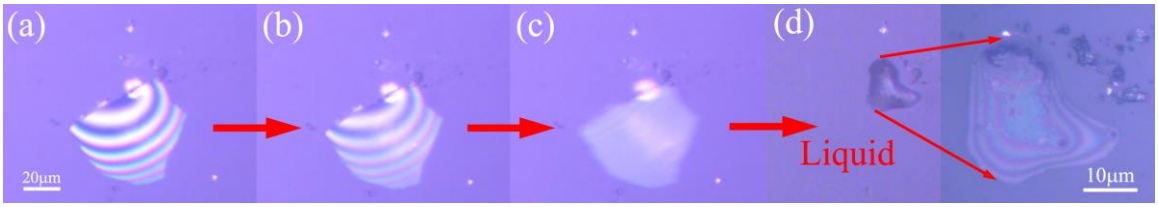

Figure.s9 demonstrated that the liquid did exist in the gap between MoS_2 membrane and glass substrate. The membrane was being taken away from original position by the probe, we can find a trace of the liquid at the position of membrane. The maximum thickness of micro-droplet was around 1μm according to the interference colors.

8. Definition and calculation details of the spatial radius (R_1 and R_2) of 3D curved membranes of Figure.3 in the main text.

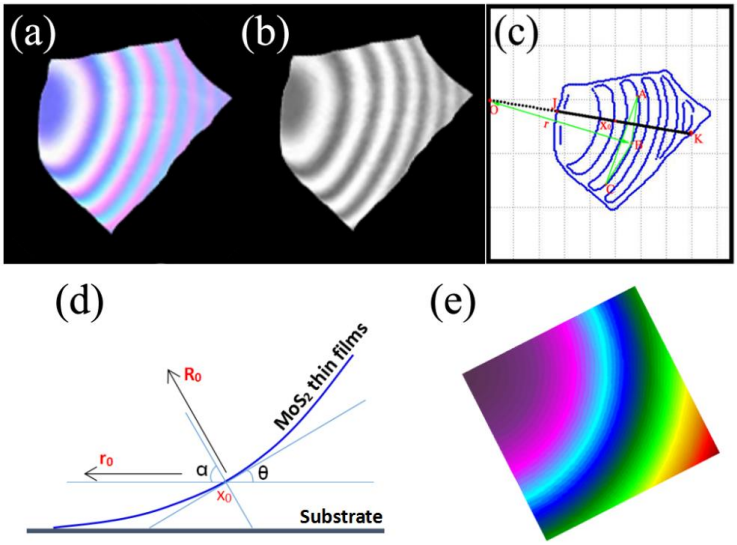

Figure.s10 is the calculation process of the curvature radius of Figure.3a in the main text. **(a)** Original image of interference colors in Figure.3a, which is anticlockwise rotated by 60°. **(b)** Grayscale image of **(a)**. **(c)** Extraction of the edge contours of interference colors from **(b)**. **(d)** The profile of the membrane at the point x_0. **(e)** The projection of simulated image onto x-y plane obtained by the fitted polynomial. All the image processing functions were semi-automatic implemented by Photoshop (Photoshop CS3) and MATLAB (MATLAB 2012b) software.

As an example, Figure.s10 shows the semi-automatic calculation process of the curvature radius R_2 in Figure.3a. Original image of interference colors in Figure.s10a is got from Figure.3a by Photoshop. A grayscale image **(b)** is transformed from Figure.s10a by using MATLAB. Then, the edge contours **(c)** are extracted through 'log' operator of MATLAB. The interference fringes are treated as a part of concentric circles. Their center is found as followed: As shown in **(c)**, three points (*A, B, C*) are selected at the edge of one fringe, and their distance (L_{AB}, L_{AC}, L_{BC}) are calculated according to the coordinates. The enclosed area can be obtained based on Heron's formula [7]:

$$S = \sqrt{P(P-L_{AB})(P-L_{AC})(P-L_{BC})}, \quad (P = \frac{L_{AB}+L_{AC}+L_{BC}}{2})$$

S is the area of triangle ΔABC, and P is the semi-perimeter of the triangle. The radius of fringes projection onto the x-y plane is allowed to be characterized by $r_0=L_{AB}L_{BC}L_{AC}/4S$. Then the coordinate of center point O can be obtained based on the radius r_0. In **(c)**, OK is an arbitrary line in 2D plane, and its position-height curve in the 3D space can be obtained as the polynomial form $z=ax^3+bx^2+cx+d$, where *a, b, c, d* are four undetermined constants. And **(d)** is the sketch of polynomial curve, x_0 is a random point on the curve. Because of the inclination angle of the wedge-shaped gap is really small (less than 2^o), the derivative is approximately equal to the sine value at x_0 point. In other words, $\tan\theta \approx \cos\alpha$. According to Meniere's theorem in differential geometry [8], the spatial radius of curvature R_2 at x_0 can be obtained as: $R_2=r_0/\cos\alpha$, while r_0 and α are shown in **(d)**.

For R_1, the position-height curve can be expand to other space after considering the formula $z=a(x^2+y^2)^{3/2}+b(x^2+y^2)+c(x^2+y^2)^{1/2}+d$, and **(e)** is the simulated image projection onto x-y plane obtained by the fitted polynomial. R_1 is given by the formula $R_1 = (1+Z'^2)^{3/2} / |Z''|$, Z is the fitted polynomial, Z' and Z'' are the first and second derivative of Z corresponding to *x, y,* respectively. And R_1 is allowed to be $R_1 = 1/|Z''|$ in the limit of $Z' << 1$.

9. Discussion of bending rigidity about the one-dimensional wrinkles.

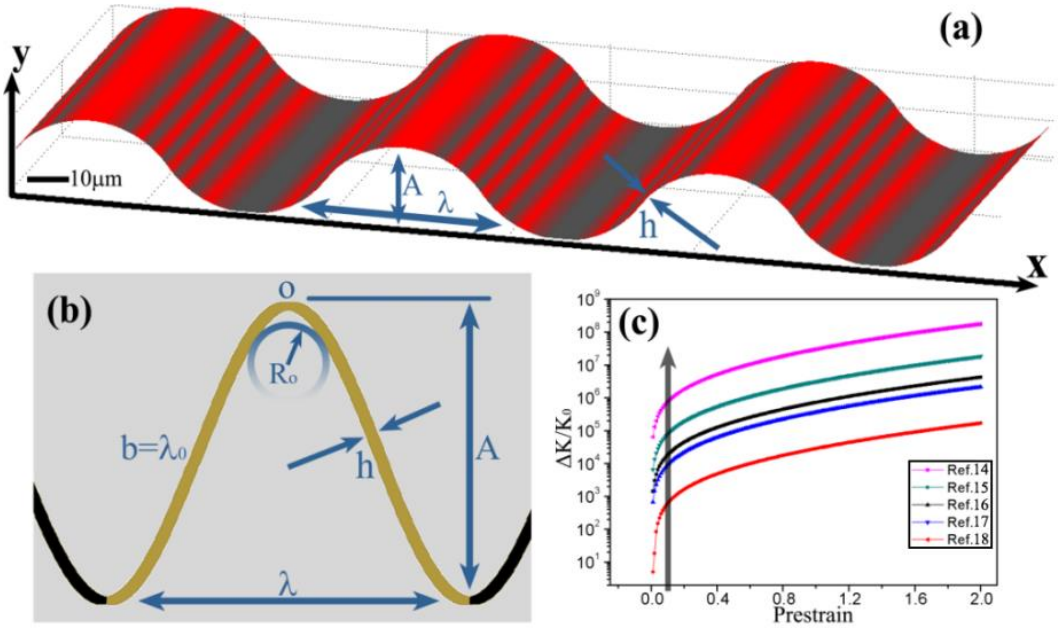

Figure.s11 (a) Simulated interference fringes of one-dimensional periodic wrinkles irradiated by a monochrome source (λ=650 nm). **(b)** The profile of wrinkles supposed to be the cosine form. **(c)** The change in stiffness of thin buckled films by changing the relaxation of the pre-stretched elastomer substrate. The parameters come from different reported references.

One-dimensional periodic wrinkles have attracted considerable research interests such as stretchable electronics [9] and energy storage [10]. By using the method provided in this work, when the magnitude A of wrinkles satisfies coherence distance of the interference (above 100 nm), the 3D structure of wrinkled films can be monitored based on interference fringes. Figure.s11(a) is simulated interferogram when irradiated by a source (λ=650 nm). As shown in **(b)**, the profile of wrinkles is represented by the cosine form in many references [11, 12], characterized by the equation as $y=A\sin(2nx/\lambda)$. The radius of curvature at peak O is given by $\kappa_0= y''(x)$ [13]。 According to the parameters of different materials provided by various literature [14-18], the change of stiffness relative to the flat state ($\Delta k/k_0$) as a function of the prestrain is shown in **(c)**. For $\varepsilon_{pre} < 10\%$, $\Delta k/k_0$ increases very sharply, then relatively gentle beyond that. And the bending stiffness could even reach 10^8 times within the literature[13] that we can find.

REFERENCES

1. Smits B. *Journal of Graphics Tools.* 1999; **4**: 11-22.
2. Fu Z, Guo F, Wong PL. *Tribology Letters*. 2008; **31**: 57-65.
3. Milgrom B, Konforti N, Golub MA, Marom E. *Optics Express.* 2010;**18**(16):17027.
4. Guo F, Wong PL. *P. I. Mech. Eng. J-J Eng.* 2002; **216:** 281-291.
5. Wang P, Xiao S, Li X, Lyu B, Huang Y, Cheng S, et al. *Scientific Reports* 2015; **5**: 18441
6. Kim Ms, Choi Jh, Park Yk. *Proc. Int. Joint Conf. SICE-ICASE. IEEE.* 2006; 2532-2537.
7. Https://en.wikipedia.org/wiki/Heron%27s_formula.
8. Mei XM, Huang J Z. *Differential geometry.* Beijing: Higher Education Press, 1988.
9. Rogers JA, Someya T, Huang, Y. *Science* 2010; **327**: 1603-1607.
10. Zang J, Cao C, Feng Y, Liu J, Zhao, X. *Sci. Rep.* 2014; **4**: 6492.
11. Vella D, Bico J, Boudaoud A, Roman B, Reis PM. *P. Natl. Acsd. Sci. USA* 2009; **106**: 10901.
12. Song J, Jiang H, Liu ZJ, Khang DY, Huang Y, Rogers JA, et al. *Int. J. Solods Struct.* 2008; **45**: 3107-3121.
13. Khang DY, Jiang H, Huang Y, Rogers JA. *Science* 2006; **311**: 208.
14. Zang J, Seunghwa R, Nicola P, Wang Q, Tu Q, Buehler MJ, et al. *Nat. Mater.* 2013; **12**: 321.
15. Cao C, Chan HF, Zang J, Leong KW, Zhao X. *Adv. Mater.* 2014; **26**: 1763-1770.
16. Wang Z, Tonderys D, Leggett SE, Williams EK, Kiani MT, Steinberg RS, et al. *Carbon* 2016; **97**: 14-24.
17. Jiang H, Khang DY, Song J, Sun Y, Huang Y, Rogers JA. *P. Natl. Acsd. Sci. USA* 2007; **104**: 15607-15612.
18. Chen PY, Sodhi J, Qiu Y, Valentin TM, Steinberg RS, Wang Z, et al. *Adv. Mater.* 2016; **28**: 3564-3571